Research Square

Preprints are preliminary reports that have not undergone peer review.
They should not be considered conclusive, used to inform clinical practice,
or referenced by the media as validated information.

# Limited Intrinsic $CO_2/CH_4$ Selectivity in Imine-Linked COF-LZU- 1: Evidence from PBE-D3 Adsorption Energetics and Binary- Mixture Monte Carlo Simulations

**Md. Kamrul Hasan**

kamrul.1913067@student.brur.ac.bd

Begum Rokeya University

**Research Article**

**Keywords:** covalent organic frameworks, COF-LZU1, $CO_2/CH_4$ separation, grand canonical Monte Carlo, density functional theory, DFT-D3, adsorption selectivity, pore filling

**Posted Date:** November 20th, 2026

**DOI:** https://doi.org/10.21203/rs.3.rs-11632627/v1

**License:** This work is licensed under a Creative Commons Attribution 4.0 International License.
Read Full License

**Additional Declarations:** No competing interests reported.

# Limited Intrinsic $CO_2/CH_4$ Selectivity in Imine-Linked COF-LZU-1: Evidence from PBE-D3 Adsorption Energetics and Binary-Mixture Monte Carlo Simulations

**Md. Kamrul Hasan**

Department of Chemistry, Begum Rokeya University, Rangpur, Bangladesh

*Corresponding author: e-mail: kamrul.1913067@student.brur.ac.bd, ORCID: 0009-0006-9528-3091.

## Abstract

Imine-linked covalent organic frameworks (COFs) are widely proposed for $CO_2/CH_4$ separation, yet the intrinsic selectivity of the archetypal framework COF-LZU1 has not been quantified against a transparent baseline. Here, periodic PBE-D3 calculations and grand canonical Monte Carlo (GCMC) simulations are combined to test whether pristine COF-LZU1 discriminates between $CO_2$ and $CH_4$. At three positions spanning the 1.8 nm channel, relaxed PBE-D3 adsorption energies are −3.10, −3.66, and −8.90 kJ $mol^{-1}$ for $CO_2$ and −3.13, −3.63, and −8.76 kJ $mol^{-1}$ for $CH_4$; $CO_2$ binds more strongly than $CH_4$ by at most 0.14 kJ $mol^{-1}$, at the confined site near the imine linkage. Consistently, GCMC simulations of equimolar mixtures (TraPPE, DREIDING, DDEC6 charges, Ewald electrostatics, 14 Å cutoff with analytic tail corrections) give low selectivities of 1.15–1.71 between 273 and 323 K and 0.1–10 bar, and 1.20–1.38 at 298 K, rising with pressure and falling with temperature. At 223 K and 7–10 bar, $CO_2$ fills about 80% of the pore volume and the selectivity reaches about 11, a pore-filling effect and not intrinsic discrimination. Replacing EPM2 $CO_2$, a 12 Å cutoff, and no tail corrections by the final force-field set raises the selectivity by 7–27%, so selectivities near unity are force-field sensitive. The weak simulated selectivity, together with the near-equal DFT binding energies, defines a baseline that functionalization, for example with $Ag^+$, must overcome.

**Keywords:** covalent organic frameworks; COF-LZU1; $CO_2/CH_4$ separation; grand canonical Monte Carlo; density functional theory; DFT-D3; adsorption selectivity; pore filling

## 1. Introduction

Removing $CO_2$ from $CH_4$-rich streams such as natural gas and biogas is required to meet pipeline and fuel specifications and to limit corrosion in transport and processing equipment. Aqueous amine scrubbing is the incumbent technology, but its solvent-regeneration energy demand and solvent degradation motivate

alternatives (1). Physisorbents are attractive because they can be regenerated by modest pressure or temperature swings, provided that they combine usable capacity with adequate $CO_2/CH_4$ selectivity.

Covalent organic frameworks (COFs) are crystalline porous polymers assembled from light elements through strong covalent bonds (2). COF-LZU1, formed by imine condensation of 1,3,5-triformylbenzene with 1,4-diaminobenzene, has hexagonal one-dimensional channels of about 1.8 nm and was first reported as a support for Pd catalysis (3). Because these channels are wide compared with $CO_2$ (kinetic diameter about 3.3 Å) and $CH_4$ (about 3.8 Å), any $CO_2/CH_4$ selectivity must arise from differences in binding energy and not from molecular sieving.

Selectivity in COF-LZU1 can be raised substantially by chemical modification: $Ag^+$-functionalized COF-LZU1 was reported to reach a $CO_2/CH_4$ selectivity of 32.1 at 298 K and 1 atm, with stable breakthrough performance over three cycles (4). Stacking also matters: combined experiments and simulations on COF-LZU1 indicated that shifted layers describe $CO_2$ uptake better than perfectly eclipsed stacking (5), and layer slipping has been examined for $CO_2/CH_4$ separation in other COFs (6). Pore-wall functionalization and multiscale screening have been used to study $CH_4/CO_2$ and $CH_4$ purification in COFs (7, 8), COF-based membranes have been developed for $CO_2/CH_4$ separation (9, 10), and the computational literature has recently been reviewed (11).

What remains missing is a transparent baseline for the pristine, eclipsed framework: whether its binding sites discriminate between $CO_2$ and $CH_4$ at all, what mixture selectivity follows over a range of temperatures and pressures, and how sensitive that selectivity is to force-field choices. Such a baseline is needed to judge what functionalization or stacking control must overcome. To the authors' knowledge, a combined site-resolved quantum-mechanical and mixture-level baseline of this kind has not been reported for COF-LZU1.

This work tests a simple hypothesis: if the quantum-mechanical binding energies of $CO_2$ and $CH_4$ at the sites available in the channel are nearly equal, the equilibrium mixture selectivity of the pristine framework must be low. The hypothesis is examined in three steps (Figure 1). Periodic PBE-D3 calculations give relaxed adsorption energies of both gases at three positions spanning the channel. DDEC6 partial charges are derived for the framework. GCMC simulations of equimolar $CO_2/CH_4$ mixtures at 223, 273, 298, and 323 K and 0.1–10 bar then give the mixture selectivity, and its sensitivity to the force-field set is quantified.

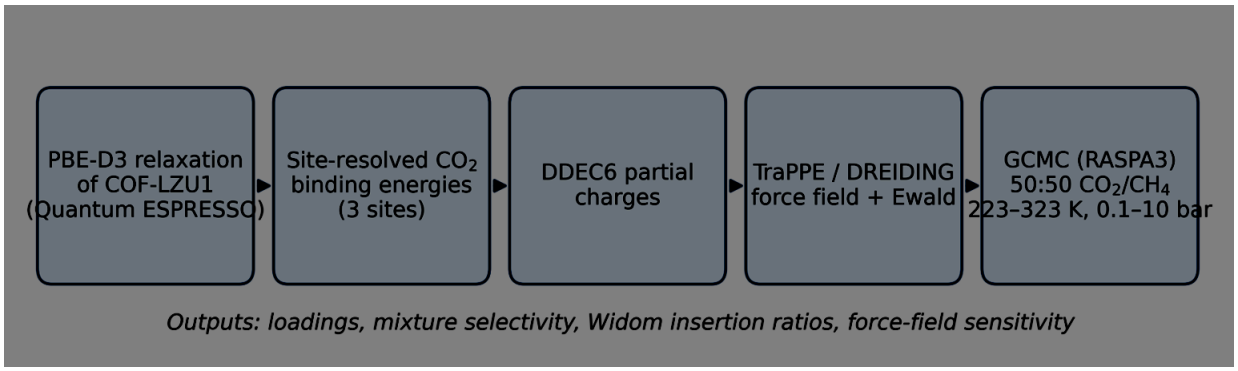



**Figure 1.** Computational workflow of this study.

## 2. Computational Methods

### 2.1 Structural model and periodic DFT

The initial structure of COF-LZU-1 was derived from the crystallographic structure associated with Cambridge Crystallographic Data Centre (CCDC) deposition 2099305 and processed to construct an eclipsed (AA-stacked) single-layer hexagonal unit cell. The resulting cell was represented in the P1 space group with lattice parameters (a = b = 22.040 Å, c = 3.729 Å, γ = 120°). The cell contains 66 atoms ($C_{36}H_{24}N_6$, 540.63 g mol$^{-1}$, volume 1568.7 Å$^3$, density 0.572 g cm$^{-3}$). Atomic positions were optimized using the BFGS algorithm in Quantum ESPRESSO while keeping the lattice parameters fixed.

Calculations used Quantum ESPRESSO v6.7MaX (12, 13) with the PBE functional (14) and the Grimme D3 dispersion correction (15) in its zero-damping form (dftd3_version = 3), with the three-body (Axilrod–Teller–Muto) term enabled. Electron–ion interactions were described with pslibrary pseudopotentials (16): C.pbe-n-kjpaw_psl.1.0.0 and O.pbe-n-kjpaw_psl.0.1 (PAW), H.pbe-rrkjus_psl.1.0.0 (ultrasoft), and N.pbe-n-radius_5.UPF (ultrasoft pseudopotential, generated using the atomic code by A. Dal Corso v5.1; author field "ivca," dated 11 December 2014). The nitrogen pseudopotential is distributed in the SSSP 1.3.0 data package. Plane-wave cutoffs were 60 Ry (wavefunctions) and 480 Ry (charge density). The Brillouin zone of the framework was sampled with a 1×1×4 Monkhorst–Pack mesh (3 irreducible k points); isolated $CO_2$ and $CH_4$ molecules were calculated in separate cubic cells with a lattice parameter of 20 Å, using Γ-point sampling. SCF energies were converged to $10^{-8}$ Ry. Ionic positions were optimized using the BFGS algorithm at fixed cell parameters, with convergence thresholds of ($10^{-4}$) Ry for total-energy changes and ($10^{-3}$) Ry/Bohr for residual forces. The relaxed pristine framework has E(COF) = −812.93557517 Ry.

### 2.2 Site-resolved adsorption energies

Three positions were selected from a two-dimensional scan of the channel (Cartesian coordinates in the cell: Site 1 (0.000, 0.000, 1.8645) Å; Site 2 (2.535, 1.622, 1.8645) Å; Site 3 (0.000, 6.013, 0.5000) Å). The corresponding local clearances were 8.86, 6.28, and 4.06 Å, respectively, where in-plane clearance denotes the minimum distance from a scan point to the framework atoms considered in the scan. $CO_2$ and $CH_4$ molecules were initially placed at the same three candidate sites, and the resulting host–guest structures were optimized using the Broyden–Fletcher–Goldfarb–Shanno (BFGS) algorithm. The atomic-position flags in the examined Quantum ESPRESSO input files indicate that both framework and guest atoms were allowed to relax during the geometry optimization

The adsorption energy is

$$E_{\mathrm{ads}} = E_{\mathrm{COF+guest}} - E_{\mathrm{COF}} - E_{\mathrm{guest}}$$

with E($CO_2$) = −101.77591667 Ry (a single SCF calculation at the fixed TraPPE geometry, C=O = 1.160 Å, relaxed) and E($CH_4$) = −23.20422180 Ry (relaxed). Energies were converted with 1 Ry = 13.605693 eV = 1312.75 kJ $mol^{-1}$. No counterpoise correction was applied. In a plane-wave basis the basis set is defined by the cell and cutoff and not by atom-centred functions, so basis-set superposition error in the usual sense does not arise.

### 2.3 Partial charges

Net atomic charges were calculated using the DDEC6 method (17) implemented in Chargemol 3.5. The calculation used the valence_density.cube electron-density file and a job_control.txt file specifying a net charge of 0.0, three-dimensional periodic boundary conditions, and the DDEC6 charge method. The atomic reference densities were obtained from the Chargemol atomic densities directory, with core-electron counts of 0 for H, 2 for C, and 2 for N. The resulting 66 atomic charges summed to approximately $+5 \times 10^{-6}$ e per unit cell and were used without subsequent neutralization. The individual atomic charges are reported in Section 3.1.

### 2.4 Force field

Framework Lennard-Jones (LJ) parameters were taken from DREIDING (18). $CO_2$ was described by the rigid, three-site TraPPE model (C=O distance 1.16 Å, q(C) = +0.70 e, q(O) = −0.35 e) (19), and $CH_4$ by the single-site TraPPE united-atom model (20). Unlike-pair LJ interactions followed Lorentz–Berthelot combining rules. The framework was held rigid (Table 1).

**Table 1.** Force-field parameters used in the GCMC simulations.

| Site | $\varepsilon/k_B$ (K) | σ (Å) | q (e) | Source |
|---|---|---|---|---|
| C (framework) | 47.871 | 3.473 | DDEC6 | DREIDING (18) |
| N (framework) | 38.961 | 3.2625 | DDEC6 | DREIDING (18) |
| H (framework) | 7.651 | 2.846 | DDEC6 | DREIDING (18) |
| $CH_4$ (united atom) | 148.0 | 3.73 | 0 | TraPPE-UA (20) |
| C ($CO_2$) | 27.0 | 2.80 | +0.70 | TraPPE (19) |
| O ($CO_2$) | 79.0 | 3.05 | −0.35 | TraPPE (19) |

## 2.5 GCMC simulations

Simulations used RASPA3 version 3.0.29 (21) for equimolar (y = 0.5) $CO_2/CH_4$ gas phases. A 2×2×8 supercell (44.08 × 44.08 × 29.83 Å, 2112 atoms, 17,300.2 g $mol^{-1}$) was used so that all perpendicular cell widths exceed twice the 14 Å cutoff. LJ interactions were truncated and shifted at 14 Å with analytic tail corrections. Electrostatics used Ewald summation with a relative precision of $10^{-6}$ (α = 0.2110 $Å^{-1}$, 9×9×7 reciprocal vectors).

Gas-phase fugacities were obtained from the Peng–Robinson equation of state (22) using $T_c$ = 304.1282 K, $p_c$ = 7.3773 MPa, ω = 0.22394 for $CO_2$ and $T_c$ = 190.564 K, $p_c$ = 4.5992 MPa, ω = 0.01142 for $CH_4$, with the binary interaction parameter taken as zero. The coefficients at each state point are in Table S1. Trial moves were translation, rotation, reinsertion, and molecule swap (insertion/deletion), with relative weights 0.5 : 0.5 : 0.5 : 1.0 per component, plus Widom test insertions. Each state point used 15,000 initialization and 25,000 production cycles from an empty framework, where a cycle consists of max(20, N) trial moves. Random seeds were generated at startup and recorded in each output file. All reported uncertainties represent standard errors calculated using RASPA3's block-averaging method over 5 equal blocks (5,000 production cycles per block. The state point at 223 K and 10.13 bar was rerun with user-specified fugacity coefficients ($CO_2$ 0.8786, $CH_4$ 0.9509; Section 3.5)

State points were T = 223, 273, 298, and 323 K and total pressures of 10,132, 101,325, 700,000, and 1,013,250 Pa (0.101, 1.013, 7.00, and 10.13 bar). The helium void fraction, from Widom insertion of helium ($\varepsilon/k_B$ = 10.9 K, σ = 2.64 Å) at 298 K, is 0.573, corresponding to a pore volume of about 1.00 $cm^3$ $g^{-1}$; it was used only to convert between absolute and excess loadings. All loadings and selectivities reported here are absolute.

## 2.6 Analysis

The adsorption selectivity of $CO_2$ over $CH_4$ is

$$S = \frac{q_{CO_2}/q_{CH_4}}{y_{CO_2}/y_{CH_4}}$$

which reduces to $q(CO_2)/q(CH_4)$ at y = 0.5. A second measure, S(W), is the ratio of the apparent Henry coefficients from Widom insertions at the state point; it equals the infinite-dilution Henry selectivity only in the low-loading limit. Uncertainties in S propagate in quadrature from the block-average errors:

$$\delta S = S\sqrt{(\frac{\delta q_{CO_2}}{q_{CO_2}})^2 + (\frac{\delta q_{CH_4}}{q_{CH_4}})^2}$$

At 0.1 bar the mean occupancy of the supercell is only about 0.3–2 molecules, so S(W), which uses many insertion attempts per cycle, is the more precise measure there.

### 2.7 Consistency checks

Four checks were made. (i) The perpendicular widths of the supercell (38.2 Å in-plane, 29.8 Å along c) exceed twice the 14 Å cutoff. (ii) The DDEC6 charges are neutral to $5\times10^{-6}$ e. (iii) In an earlier run set with a different force field, independent simulations with 85,000 and 40,000 total cycles at 223 K gave S = 1.28 ± 0.05 and 1.29 ± 0.06 at 0.1 bar and 1.37 ± 0.06 and 1.38 ± 0.05 at 1 bar, i.e. agreement within errors. (iv) A separate implementation of the Peng–Robinson equation (script provided in the Supporting Information) reproduced RASPA3's fugacity coefficients at 298 K and 10.13 bar and at 223 K and 7 bar to four decimals; this check also exposed a discrepancy at 223 K and 10.13 bar (Section 3.5).

## 3. Results and Discussion

### 3.1 Framework partial charges

The The DDEC6 partial charges on the framework atoms are relatively small (Table 2, Figure 2), ranging from -0.294 e on the six imine nitrogen atoms to +0.209 e on the most positive carbon atom, while hydrogen charges lie between +0.051 e and +0.104 e (maintaining overall unit cell neutrality). With $|q| \leq 0.294$ e, the electric field inside the framework pores is weak, suggesting that electrostatic interactions contribute minimally to quadrupolar $CO_2$ adsorption compared to van der Waals forces. This is consistent with previous findings for COF-LZU1, where neglecting framework partial charges modified $CO_2$ uptake by less than 7% (5).

**Table 2.** DDEC6 net atomic charges of the 66-atom cell, grouped by label (all groups contain six atoms; values are group means; the spread within each group is below 0.0001 e).

| Label group | Element | q (e) | Tentative environment |
|---|---|---|---|
| C1–C6 | Carbon | +0.0581 | aromatic C bonded to the imine carbon |
| C7–C12 | Carbon | −0.1251 | aromatic C–H, triformylbenzene ring |
| C13–C18 | Carbon | +0.0890 | aromatic C bonded to N |
| N19–N24 | Nitrogen | −0.2935 | imine N |

| Label group | Element | q (e) | Tentative environment |
|---|---|---|---|
| C25–C30 | Carbon | +0.2085 | imine C |
| C31–C36 | Carbon | -0.1277 | aromatic C–H, phenylene ring |
| C37-C42 | Carbon | -0.1586 | aromatic C–H, phenylene ring |
| H43–H48 | Hydrogen | +0.0964 | H, triformylbenzene ring |
| H49–H54 | Hydrogen | +0.0506 | H, phenylene ring (site 1) |
| H55–H60 | Hydrogen | +0.1043 | imine H |
| H61–H66 | Hydrogen | +0.0979 | H, henylene ring (site 2) |

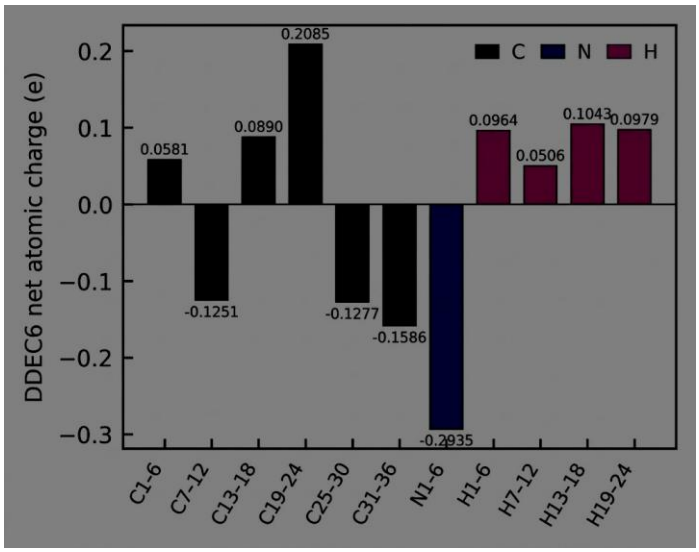



**Figure 2.** DDEC6 net atomic charges by label group.

### 3.2 $CO_2$ and $CH_4$ binding at three sites from PBE-D3

The relaxed PBE-D3 adsorption energies (Table 3, Figure 3) show weak physisorption of both gases and, more importantly, no meaningful preference of the framework for either. At the pore centre (Site 1) $CO_2$ and $CH_4$ bind with −3.10 and −3.13 kJ mol$^{-1}$; at the intermediate Site 2 with −3.66 and −3.63 kJ mol$^{-1}$; and at the confined Site 3, 4.06 Å from the nearest framework atom, with −8.90 and −8.76 kJ mol$^{-1}$. The largest difference, 0.14 kJ mol$^{-1}$ at Site 3, lies below the uncertainty normally expected of PBE-D3 adsorption energies, and the corresponding Boltzmann factor at 298 K is 1.06 (0.99 and 1.01 at the other two sites).

Binding is strongest at Site 3 for both gases, 2.87 times ($CO_2$) and 2.80 times ($CH_4$) stronger than at the pore centre. Because the strengthening is the same for nonpolar $CH_4$ as for $CO_2$, it is attributed to confinement and multiple short-range dispersion contacts with the phenyl and imine groups, not to a $CO_2$-specific interaction with the imine nitrogen: such an interaction would favour $CO_2$ at Site 3.

A caveat concerns the reference energies. Isolated $CH_4$ was relaxed, whereas isolated $CO_2$ was computed at a fixed C=O distance of 1.160 Å (the TraPPE value) without relaxation. If the PBE-D3 equilibrium C=O distance is longer than 1.160 Å (PBE typically gives about 1.17 Å), the $CO_2$ reference energy is too high and the $CO_2$ adsorption energies in Table 3 are too negative by roughly 0.3–1.1 kJ mol$^{-1}$ (a harmonic estimate for a 0.005–0.010 Å difference). A correction of this size would make $CH_4$ appear to bind slightly more strongly than $CO_2$, which would reinforce, not weaken, the conclusion that the framework offers no $CO_2$ preference. Four further caveats apply: only three positions were examined and there is no thermal sampling; the single-layer cell imposes a 3.729 Å repeat along the channel; no counterpoise correction was applied; and adsorption energies are not isosteric heats, which include thermal and adsorbate–adsorbate terms.

**Table 3.** Relaxed PBE-D3 adsorption energies of $CO_2$ and $CH_4$ at three sites in COF-LZU1 (energies in eV in parentheses; total energies in Table S2). Red entries depend on the unrelaxed $CO_2$ reference energy and are provisional.

| Site | Clearance (Å) | $E_{ads}$, $CO_2$ (kJ mol$^{-1}$) | $E_{ads}$, $CH_4$ (kJ mol$^{-1}$) | $CO_2 - CH_4$ (kJ mol$^{-1}$) | Boltzmann factor, 298 K |
|---|---|---|---|---|---|
| 1 (pore centre) | 8.86 | −3.10 (−0.0322) | −3.13 (−0.0325) | +0.03 | 0.99 |
| 2 (intermediate) | 6.28 | −3.66 (−0.0379) | −3.63 (−0.0376) | −0.03 | 1.01 |
| 3 (confined) | 4.06 | −8.90 (−0.0923) | −8.76 (−0.0908) | −0.14 | 1.06 |

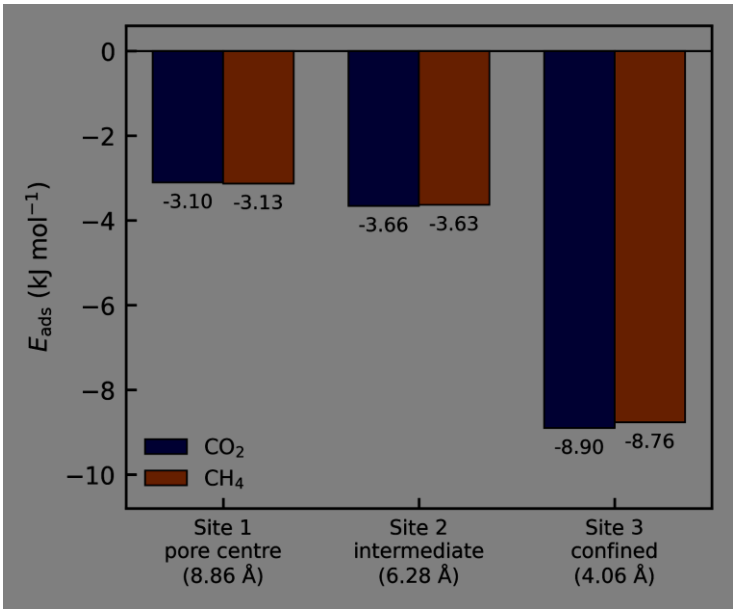



**Figure 3.** Relaxed PBE-D3 adsorption energies of $CO_2$ and $CH_4$ at the three sites. [$CO_2$ values are provisional: the isolated-$CO_2$ reference energy is being relaxed.]

### 3.3 Adsorption of $CO_2$ and $CH_4$ from equimolar mixtures

Absolute loadings from the 50:50 mixtures are listed in Table 4 and plotted in Figure 4. Loadings of both gases rise with pressure and fall with temperature. At 298 K the uptake is close to linear in pressure over the whole range ($CO_2$: 0.0207 mmol $g^{-1}$ at 0.101 bar, 0.209 at 1.01 bar, and 2.17 at 10.1 bar; $CH_4$: 0.0172, 0.169, and 1.57 mmol $g^{-1}$), so Henry's-law behaviour persists to 10 bar at this temperature; the $CO_2$ loading at 1.01 bar corresponds to about 4.7 $cm^3$(STP) $g^{-1}$. At 273 K the $CO_2$ isotherm becomes slightly superlinear (0.0328, 0.335, and 4.02 mmol $g^{-1}$), indicating cooperative adsorbate–adsorbate interactions. At 223 K the $CO_2$ loading increases about 15-fold between 1 and 7 bar (1.40 to 20.7 mmol $g^{-1}$) and then levels off at 21.2 mmol $g^{-1}$ at 10.1 bar, whereas $CH_4$ rises only from 0.81 to 1.8–2.0 mmol $g^{-1}$ (Section 3.5).

**Table 4.** GCMC results for the equimolar $CO_2/CH_4$ mixture in COF-LZU1 (absolute loadings, ± one block-average standard error; S from loadings, S(W) from Widom insertions).

| T (K) | P (bar) | q($CO_2$) (mmol $g^{-1}$) | q($CH_4$) (mmol $g^{-1}$) | S | S(W) |
|---|---|---|---|---|---|
| 223 | 0.101 | 0.119 ± 0.004 | 0.084 ± 0.001 | 1.41 ± 0.05 | 1.48 ± 0.04 |
| 223 | 1.013 | 1.398 ± 0.040 | 0.813 ± 0.019 | 1.72 ± 0.06 | 1.73 ± 0.05 |
| 223 | 7.00 | 20.74 ± 0.22 | 1.80 ± 0.08 | 11.5 ± 0.5 | 13.0 ± 2.4 |
| 223 | 10.13 | 21.82 ± 0.22 | 1.68 ± 0.17 | 12.98 ± 0.9 | 14.29 ± 2.26 |
| 273 | 0.101 | 0.0328 ± 0.0010 | 0.0266 ± 0.0004 | 1.23 ± 0.04 | 1.26 ± 0.03 |
| 273 | 1.013 | 0.335 ± 0.004 | 0.261 ± 0.010 | 1.29 ± 0.05 | 1.30 ± 0.03 |
| 273 | 7.00 | 2.570 ± 0.038 | 1.692 ± 0.017 | 1.52 ± 0.03 | 1.57 ± 0.02 |
| 273 | 10.13 | 4.020 ± 0.050 | 2.351 ± 0.014 | 1.71 ± 0.02 | 1.77 ± 0.02 |
| 298 | 0.101 | 0.0207 ± 0.0011 | 0.0172 ± 0.0004 | 1.20 ± 0.07 | 1.20 ± 0.02 |
| 298 | 1.013 | 0.209 ± 0.003 | 0.169 ± 0.004 | 1.24 ± 0.03 | 1.23 ± 0.02 |
| 298 | 7.00 | 1.466 ± 0.017 | 1.114 ± 0.010 | 1.32 ± 0.02 | 1.34 ± 0.01 |
| 298 | 10.13 | 2.165 ± 0.032 | 1.574 ± 0.010 | 1.38 ± 0.02 | 1.43 ± 0.02 |
| 323 | 0.101 | 0.0144 ± 0.0005 | 0.0125 ± 0.0005 | 1.15 ± 0.06 | 1.18 ± 0.01 |
| 323 | 1.013 | 0.142 ± 0.002 | 0.122 ± 0.003 | 1.16 ± 0.03 | 1.18 ± 0.01 |
| 323 | 7.00 | 0.953 ± 0.020 | 0.786 ± 0.014 | 1.21 ± 0.03 | 1.23 ± 0.01 |
| 323 | 10.13 | 1.395 ± 0.020 | 1.138 ± 0.011 | 1.23 ± 0.02 | 1.29 ± 0.03 |

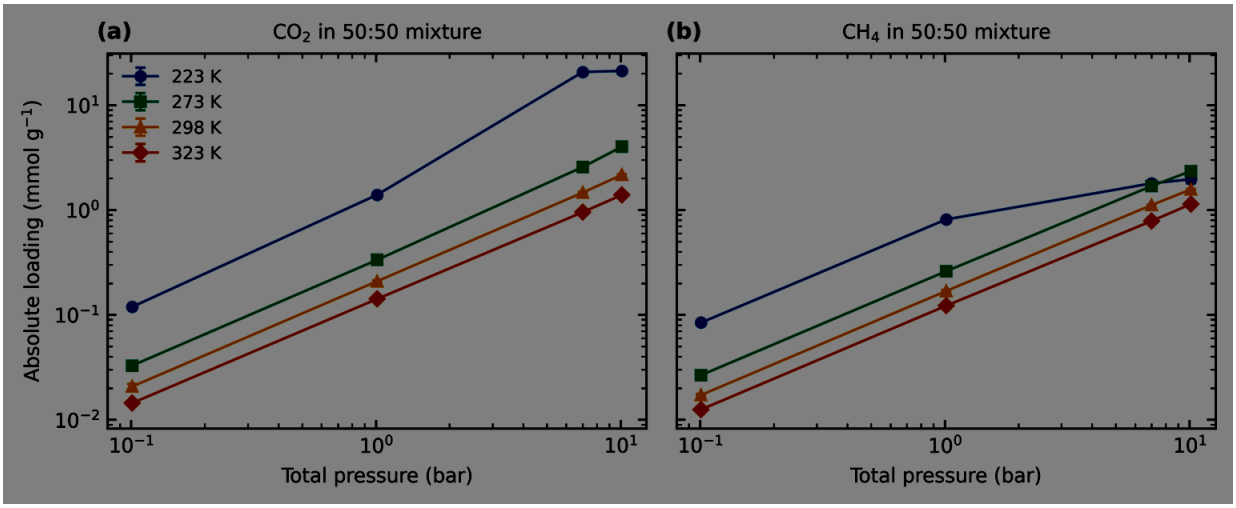



**Figure 4.** Absolute loadings of (a) $CO_2$ and (b) $CH_4$ from the 50:50 mixture. At 223 K the 7 and 10 bar points lie in the pore-filling regime.

### 3.4 Mixture selectivity

The selectivity is modest everywhere except in the pore-filling regime (Figure 5). Between 273 and 323 K, S ranges from 1.15 (323 K, 0.101 bar) to 1.71 (273 K, 10.1 bar); at 298 K it increases from 1.20 ± 0.07 at 0.101 bar to 1.38 ± 0.02 at 10.1 bar. Two trends hold at all state points: S decreases with temperature, and S increases with pressure. The pressure effect is largest at 273 K (1.23 to 1.71), where the $CO_2$ isotherm is superlinear. The Widom ratio S(W) agrees with S within about two standard errors at most state points and is slightly larger at the highest pressures (298 K, 10.1 bar: S = 1.38 ± 0.02, S(W) = 1.43 ± 0.02).

The weak simulated selectivity agrees with the DFT result of Section 3.2. At 298 K and 0.1 bar, where loadings are lowest and the system is closest to the Henry limit, S = 1.20 ± 0.07 and S(W) = 1.20 ± 0.02, compared with Boltzmann factors of 0.99–1.06 from the PBE-D3 energies. The remaining excess of the simulated value over the DFT-based factor may reflect entropic and packing contributions and differences between the classical force field and PBE-D3;

The $Ag^+$-modified COF-LZU1 was reported to reach a selectivity of 32.1 at 298 K and 1 atm (4). The pristine-framework values here (1.2–1.4 at 298 K) are more than an order of magnitude lower, although the way selectivity was defined and obtained in ref 4 (IAST, breakthrough, or mixture simulation) must be compared before a quantitative statement is made. This gap is what functionalization must close.

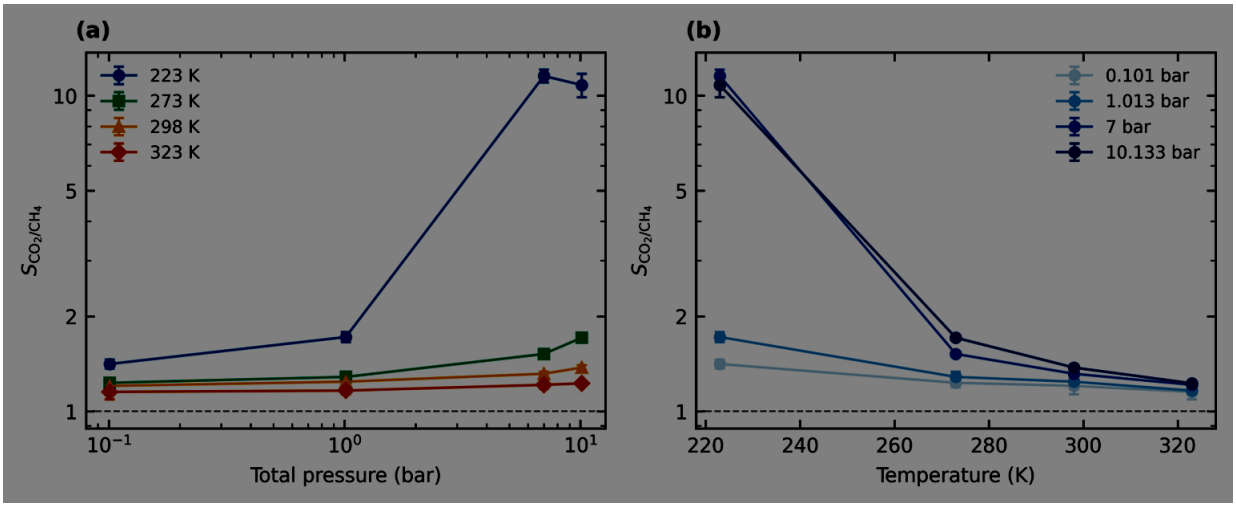



**Figure 5.** $CO_2/CH_4$ selectivity S (a) versus pressure and (b) versus temperature; error bars are one standard error.

### 3.5 Pore filling at 223 K

At 223 K and 7–10 bar, the $CO_2$ loadings of 20.7 ± 0.2 and 21.2 ± 0.2 mmol $g^{-1}$ correspond to about 0.91 g of $CO_2$ per gram of framework. At a liquid-like density of roughly 1.15 g $cm^{-3}$, this is about 0.8 $cm^3$ $g^{-1}$, or roughly 80% of the helium-accessible pore volume (1.00 $cm^3$ $g^{-1}$). The superlinear rise between 1 and 7 bar followed by saturation is characteristic of pore filling.

The bulk gas is stable as a single phase under these conditions. With the Peng–Robinson equation (binary interaction parameter zero), the pure-$CO_2$ saturation pressure at 223 K is 6.74 bar and the equimolar mixture has a dew pressure of about 14.1 bar, so the bulk mixture is a vapor at both 7 and 10.13 bar (the latter is about 72% of the dew pressure). The $CO_2$ partial pressures of 3.5 and 5.1 bar are 0.52 and 0.75 of the pure-$CO_2$ saturation pressure. The loading plateau therefore reflects condensation inside the channels and not bulk condensation .

. At 223 K and 10.13 bar, RASPA3 reported compressibilities of 0.028 for the $CO_2$ entry and 0.907 for the $CH_4$ entry, i.e. different roots of the cubic equation. The $CO_2$ fugacity coefficient of the liquid-like root or the vapor root gives 0.8786 (the $CH_4$ value, 0.9509, is the vapor-root value in both).

The selectivities in this regime (S = 12.98 ± 0.9 at 10 bar; S(W) = 14.29 ± 2.26) reflect preferential filling of the channel by condensed $CO_2$, in which $CH_4$ is a minority component (1.68 ± 0.17 mmol $g^{-1}$ at 10 bar). They should be presented as a pore-filling observation and not as evidence of high intrinsic selectivity.

### 3.6 Sensitivity to the force-field set

The sweep was first run with a different set: EPM2 $CO_2$ (q(C) = +0.6512 e), a $CH_4$ well depth of 158.5 K with σ = 3.72 Å, a 12 Å cutoff with truncation and shifting but no tail corrections, and a 2×2×7 supercell. Changing to the TraPPE/14 Å/tail-corrected set raised S at all 14 state points where both sets are available, by 7% (323 K, 1.01 bar) to 27% (273 K, 10.1 bar) (Figure 6). At 298 K and 1.01 bar, for example, S increased from 1.11 ± 0.02 to 1.24 ± 0.03, with the $CO_2$ loading rising by about 27% and the $CH_4$ loading by about 14%. Because the $CO_2$ model, the $CH_4$ well depth, and the cutoff treatment changed together, the effect cannot be attributed to any one of them. The practical point is that when intrinsic selectivities are near 1, changes of 10–25% from force-field choices are comparable to the differences between conditions, so quoted selectivities should be accompanied by the force-field specification.

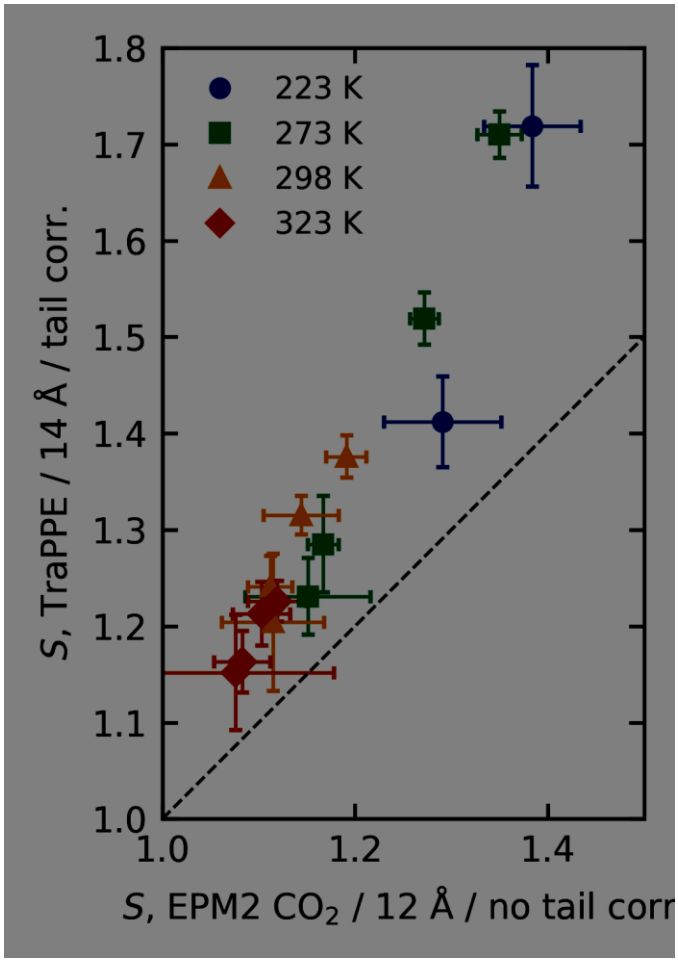



**Figure 6.** Selectivity with TraPPE/14 Å/tail corrections versus EPM2/12 Å/no tail corrections at 14 state points; the dashed line is parity.

### 3.7 Why the selectivity is low, and what it implies

Three observations point the same way. The PBE-D3 energies of $CO_2$ and $CH_4$ differ by at most 0.14 kJ $mol^{-1}$ at three sites that span the channel; the DDEC6 charges are small ($|q| \leq 0.29$ e), so the quadrupole of $CO_2$ has little electrostatic field to exploit; and the channel is far wider than either molecule, so there is no sieving. Within this model, pristine COF-LZU1 is therefore a high-capacity but low-selectivity adsorbent at moderate temperatures. Substantial gains would need strong, $CO_2$-specific sites (for example $Ag^+$, as in ref 4) or control of the pore environment, such as layer offset (5, 6) or wall functionalization (7).

The limitations are as follows. (i) The idealized eclipsed single-layer structure may bind less strongly at low pressure than the shifted structures favoured experimentally (5), so the selectivities are specific to the eclipsed model. (ii) The framework is rigid and the charges are fixed. (iii) Only equimolar feeds were studied. (iv) Water, diffusion, and kinetic effects are not included. (v) The DFT energies cover three positions.

## 4. Conclusions

Relaxed PBE-D3 calculations indicate that pristine COF-LZU1 binds $CO_2$ and $CH_4$ almost equally at three sites spanning the channel: −3.10, −3.66, and −8.90 kJ $mol^{-1}$ for $CO_2$ and −3.13, −3.63, and −8.76 kJ $mol^{-1}$ for $CH_4$. Equimolar GCMC simulations agree: the selectivity is 1.15–1.71 between 273 and 323 K and 0.1–10 bar, and 1.20–1.38 at 298 K, increasing with pressure and decreasing with temperature. At 223 K and 7–10 bar, $CO_2$ fills about 80% of the pore volume and the selectivity rises to about 13; this is a pore-filling effect. The selectivity increases by 7–27% when the force field is changed from EPM2/12 Å to TraPPE/14 Å with tail corrections. These results provide a baseline against which the gains from functionalization and stacking control can be quantified.

## Associated Content

**Supporting Information:** Supporting Information includes Tables S1 and S2; the file SI_GCMC_results_TraPPE_14A.csv, containing adsorption loadings, selectivities, and associated uncertainties; and the Python script pr_fugacity_check.py used for the fugacity calculations. Additional files provided with the Supporting Information include the COF-LZU-1 CIF structure containing DDEC6 atomic charges, force_field.json, simulation.json, and the Quantum ESPRESSO input files used for the DFT calculations. These files document the structural models, force-field parameters, simulation settings, and computational procedures used in this study.

## Author Information

**Corresponding Author:** Md. Kamrul Hasan, Department of Chemistry, Begum Rokeya University, Rangpur, Bangladesh;

E-mail: kamrul.1913067@student.brur.ac.bd

ORCID: 0009-0006-9528-3091.

**Notes:** The author declares no competing financial interests or personal relationships that could have influenced the work reported in this paper.

**Acknowledgments:** The author acknowledges the use of personal computing resources for the computational simulations and data analysis conducted in this study.

**Author contributions (CRediT):** he author was responsible for conceptualization, methodology, software, validation, formal analysis, investigation, data curation, visualization, and writing—original draft preparation and review and editing.

## References

(1) Rochelle, G. T. Amine Scrubbing for $CO_2$ Capture. *Science* **2009**, *325*, 1652–1654. DOI: 10.1126/science.1176731.

(2) Côté, A. P.; Benin, A. I.; Ockwig, N. W.; O'Keeffe, M.; Matzger, A. J.; Yaghi, O. M. Porous, Crystalline, Covalent Organic Frameworks. *Science* **2005**, *310*, 1166–1170. DOI: 10.1126/science.1120411.

(3) Ding, S.-Y.; Gao, J.; Wang, Q.; Zhang, Y.; Song, W.-G.; Su, C.-Y.; Wang, W. Construction of Covalent Organic Framework for Catalysis: Pd/COF-LZU1 in Suzuki–Miyaura Coupling Reaction. *J. Am. Chem. Soc.* **2011**, *133*, 19816–19822.

(4) Chu, J.-Q.; Song, R.; Han, Y.-J.; Wei, Q.; Han, Z.-B. Silver(I)-Functionalized COF-LZU1 for High-Performance $CO_2/CH_4$ Separation. *Inorganic Chemistry* **2025**, *64* (19), 9907–9911. https://doi.org/10.1021/acs.inorgchem.5c01584.

(5) Kessler, C.; Schuldt, R.; Emmerling, S.; Lotsch, B. V.; Kästner, J.; Gross, J.; Hansen, N. Influence of Layer Slipping on Adsorption of Light Gases in Covalent Organic Frameworks: A Combined Experimental and Computational Study. *Microporous and Mesoporous Materials* **2022**, *336*, 111796. https://doi.org/10.1016/j.micromeso.2022.111796.

(6) Sharma, A.; Babarao, R.; Medhekar, N. V.; Malani, A. Methane Adsorption and Separation in Slipped and Functionalized Covalent Organic Frameworks. *Industrial & Engineering Chemistry Research* **2018**, *57* (14), 4767–4778. https://doi.org/10.1021/acs.iecr.7b05031.

(7) Fang, Z.; Wang, C.; Li, C.; Li, X.; Feng, X.; Zhang, L.; Li, H. Improved Selectivity of $CH_4/CO_2$ within 1D Channel of COFs Realized by Pore Wall Functionalization Strategy. *Nano Research* **2026**, *19* (3), 94908269. https://doi.org/10.26599/NR.2025.94908269.

(8) Altundal, Ö. F.; Haslak, Z. P.; Keskin, S. Combined GCMC, MD, and DFT Approach for Unlocking the Performances of COFs for Methane Purification. *Industrial & Engineering Chemistry Research* **2021**, *60* (35), 12999–13012. https://doi.org/10.1021/acs.iecr.1c01742.

(9) Fan, H.; Mundstock, A.; Gu, J.; Meng, H.; Caro, J. An Azine-Linked Covalent Organic Framework ACOF-1 Membrane for Highly Selective $CO_2/CH_4$ Separation. *Journal of Materials Chemistry A* **2018**, *6* (35), 16849–16853. https://doi.org/10.1039/C8TA05641B.

(10) Shan, M.; Seoane de la Cuesta, B.; Rozhko, E.; Dikhtiarenko, A.; Clet, G.; Kapteijn, F.; Gascon, J. "Azine-Linked Covalent Organic Framework (COF)-Based Mixed-Matrix Membranes for $CO_2/CH_4$ Separation." Chemistry – A European Journal 2016, 22(41), 14467–14470. https://doi.org/10.1002/chem.201602999.

(11) Rajguru, P.; Bora, P.; Bhuyan, C.; Hazarika, S. "Exploring Covalent Organic Frameworks through the Lens of Computational Chemistry." Materials Advances 2026, 7(2), 682–714. https://doi.org/10.1039/D5MA00843C

(12) Giannozzi, P.; et al. QUANTUM ESPRESSO: A Modular and Open-Source Software Project for Quantum Simulations of Materials. *J. Phys.: Condens. Matter* **2009**, *21*, 395502.

(13) Giannozzi, P.; et al. Advanced Capabilities for Materials Modelling with Quantum ESPRESSO. *J. Phys.: Condens. Matter* **2017**, *29*, 465901.

(14) Perdew, J. P.; Burke, K.; Ernzerhof, M. Generalized Gradient Approximation Made Simple. *Phys. Rev. Lett.* **1996**, *77*, 3865–3868.

(15) Grimme, S.; Antony, J.; Ehrlich, S.; Krieg, H. A Consistent and Accurate Ab Initio Parametrization of Density Functional Dispersion Correction (DFT-D) for the 94 Elements H–Pu. *J. Chem. Phys.* **2010**, *132*, 154104.

(16) Dal Corso, A. Pseudopotentials Periodic Table: From H to Pu. *Comput. Mater. Sci.* **2014**, *95*, 337–350.

(17) Manz, T. A.; Limas, N. G. Introducing DDEC6 Atomic Population Analysis: Part 1. Charge Partitioning Theory and Methodology. *RSC Adv.* **2016**, *6*, 47771–47801. Chargemol program, version 3.5.

(18) Mayo, S. L.; Olafson, B. D.; Goddard, W. A. DREIDING: A Generic Force Field for Molecular Simulations. *J. Phys. Chem.* **1990**, *94*, 8897–8909.

(19) Potoff, J. J.; Siepmann, J. I. Vapor–Liquid Equilibria of Mixtures Containing Alkanes, Carbon Dioxide, and Nitrogen. *AIChE J.* **2001**, *47*, 1676–1682.

(20) Martin, M. G.; Siepmann, J. I. Transferable Potentials for Phase Equilibria. 1. United-Atom Description of n-Alkanes. *J. Phys. Chem. B* **1998**, *102*, 2569–2577.

(21) Dubbeldam, D.; Calero, S.; Ellis, D. E.; Snurr, R. Q. RASPA: Molecular Simulation Software for Adsorption and Diffusion in Flexible Nanoporous Materials. *Mol. Simul.* **2016**, *42*, 81–101. RASPA3 version 3.0.29.

(22) Peng, D.-Y.; Robinson, D. B. A New Two-Constant Equation of State. *Ind. Eng. Chem. Fundam.* **1976**, *15*, 59–64.

## Supporting Information (draft)

**Table S1.** Peng–Robinson fugacity coefficients and compressibility factors of the equimolar mixture, as reported by RASPA3 ($k_{ij} = 0$).

| T (K) | P (bar) | φ($CO_2$) | φ($CH_4$) | Z (mixture) |
|---|---|---|---|---|
| 223 | 0.101 | 0.9988 | 0.9995 | 0.9991 |
| 223 | 1.013 | 0.9876 | 0.9949 | 0.9912 |
| 223 | 7.00 | 0.9156 | 0.9656 | 0.9372 |
| 223 | 10.13 | 0.8786 | 0.9509 | 0.4678 |
| 273 | 0.101 | 0.9993 | 0.9997 | 0.9995 |
| 273 | 1.013 | 0.9930 | 0.9972 | 0.9951 |
| 273 | 7.00 | 0.9522 | 0.9810 | 0.9657 |
| 273 | 10.13 | 0.9311 | 0.9728 | 0.9501 |
| 298 | 0.101 | 0.9995 | 0.9998 | 0.9996 |
| 298 | 1.013 | 0.9946 | 0.9979 | 0.9962 |
| 298 | 7.00 | 0.9631 | 0.9857 | 0.9739 |
| 298 | 10.13 | 0.9468 | 0.9794 | 0.9622 |
| 323 | 0.101 | 0.9996 | 0.9998 | 0.9997 |
| 323 | 1.013 | 0.9958 | 0.9984 | 0.9971 |
| 323 | 7.00 | 0.9712 | 0.9891 | 0.9799 |
| 323 | 10.13 | 0.9585 | 0.9843 | 0.9709 |

**Table S2.** Quantum ESPRESSO total energies (Ry).

| System | Energy (Ry) |
|---|---|
| COF-LZU1 (relaxed) | −812.93557517 |
| $CO_2$ (isolated; fixed C=O = 1.160 Å) | −101.77591667 |
| $CH_4$ (isolated; relaxed) | −23.20422180 |
| COF + $CO_2$, Site 1 | −914.71385563 |
| COF + $CO_2$, Site 2 | −914.71427713 |
| COF + $CO_2$, Site 3 | −914.71827236 |
| COF + $CH_4$, Site 1 | −836.14218305 |
| COF + $CH_4$, Site 2 | −836.14256349 |
| COF + $CH_4$, Site 3 | −836.14647320 |

# TOC graphic

